Journal of Power Sources 260 (2014) 19–26

Contents lists available at ScienceDirect

Journal of Power Sources

journal homepage: www.elsevier.com/locate/jpowsour

A 4 V-electrochemical capacitor using electrode and electrolyte materials free of metals

Cheng Zheng [a,b], Masaki Yoshio [c], Li Qi [a], Hongyu Wang [a,*]

[a] State Key Laboratory of Electroanalytical Chemistry, Changchun Institute of Applied Chemistry, Chinese Academy of Sciences, 5625 Renmin Street, Changchun 130022, China
[b] University of Chinese Academy of Sciences, Beijing 100049, China
[c] Advanced Research Center, Saga University, 1341 Yoga-machi, Saga 840-0047, Japan

HIGHLIGHTS

- MCMBs as electrodes for 4 V electrochemical capacitors using metal-free electrolytes.
- Electrochemical activation has big influence on activated MCMB negative electrode.
- Both energy and power densities of a capacitor are elevated remarkably.

ARTICLE INFO

Article history:
Received 3 January 2014
Accepted 25 February 2014
Available online 14 March 2014

Keywords:
Electrochemical capacitors
Mesophase carbon microbeads
Non-porous activated soft carbon
Electrochemical activation
Quaternary alkyl ammonium

ABSTRACT

A 4 V asymmetric capacitor has been assembled using non-porous activated mesophase carbon microbeads (AMCMB) as the negative electrode, a graphitized carbon (GMCMB) as the positive electrode and quaternary alkyl ammonium based organic electrolyte. AMCMB has been heated under the reduction atmosphere of hydrogen/nitrogen after a chemical activation. It has small specific surface area (24.48 $m^2 g^{-1}$), but delivers a large capacitance value due to the irreversible "electrochemical activation" in the initial galvanostatic charge–discharge process. The storage charge behavior of AMCMB has also been investigated by *ex situ* XRD, Raman spectroscopy, cyclic voltammetry and electrochemical impedance spectroscopy. In terms of specific capacity, energy density, power density and cycle ability, the AMCMB/GMCMB capacitor is superior the other capacitors like AC/graphite, AC/AC.

1. Introduction

Recently, electrochemical capacitors have attracted the research interest all over the world and many progresses have been published. But the social needs of human being will continuously put forward new criteria accessing this kind of electric energy storage devices. For instance, elevating their energy density to over 20 Wh kg^{-1} without sacrificing most of their traditional traits is still a big challenge [1]. To ensure both high energy and power densities, the working voltage of an electrochemical capacitor must be lifted at first. Until now, strategies to widen the working voltage range include the choice of non-aqueous electrolytes and the assembly of asymmetric capacitors consisting of battery-type electrode materials. Most high-voltage electrochemical capacitors have been summarized in a recent review [2]. Intriguingly, many such capacitors utilize non-aqueous lithium-ion electrolytes and lithium-storage electrode materials, which belong to "lithium-ion capacitors". Whether in lithium-ion batteries or capacitors, these materials actually share the same charge carrier (lithium ion) and involve similar charge storage mechanisms. Therefore, most lithium-ion capacitors inherit the ill genes of lithium-ion batteries. For example, a negative electrode of lithium-doped carbon is liable to lithium metal deposition during the charge process in cold environments [3], while the negative electrode of $Li_4T_5O_{12}$ is likely to trigger electrolytes decomposition and liberate considerable amounts of gas at high temperatures [4,5]. Consequently, the lithium-ion capacitors using the above negative electrodes have the risk of safety problems. On the other hand, in some lithium-ion capacitors using lithium-storage positive electrode materials, porous carbons are usually employed as negative electrode materials, which accumulate the heavily solvated lithium ions instead of the "bare" ones. The high surface area of porous carbon has a high

* Corresponding author. Tel./fax: +86 431 85262287.
E-mail addresses: hongyuwang@ciac.ac.cn, hongyuwang@aliyun.com (H. Wang).

http://dx.doi.org/10.1016/j.jpowsour.2014.02.098
0378-7753/

catalytic activity, so the organic solvent together with lithium ions intruding into the pores of carbon electrodes can be noticeably reduced at low potentials. Thus the reduction products block the pores and deteriorate the performance of capacitors at last [6,7].

To escape from the embarrassing circumstances of lithium-ion capacitors, an alternative way turns to the energy storage devices based on non-metal ions. Commercial electric double-layer capacitors (EDLCs) are the prototype of such a concept, which comprise two symmetrical porous carbon electrodes and the organic solution dissolving a quaternary alkyl ammonium salt. In fact, some of their merits have not drawn enough attention yet. For example, the utilization of Al current (instead of Cu) collectors can cut both the weight and cost of a capacitor. Heavy metals are not present in the electrode materials and electrolytes, which virtue is economically and ecologically advantageous for recycling treatments. Until now, most of the research interest on EDLCs has been focused on how to increase their gravimetric capacitance values by enlarging the specific surface area and tailoring the pore size of carbon electrode materials. However, the exaggeration of porosity's role may results in a light tap density of carbon electrode and a low volumetric capacitance in the practical capacitors [8]. On the other hand, a porous carbon abounds in active functional groups on the surface, which easily lead to electrolytes decomposition in the high voltage range of a capacitor [9]. So the voltage of EDLCs is generally limited to 2.7 V, even using stable non-aqueous electrolytes.

Therefore, to further raise the voltage of capacitors using quaternary alkyl ammonium-based organic electrolytes, the electrode/electrolyte interface must be restricted. Decreasing the surface area of carbon electrode can effectively suppress the electrolytes decomposition. Some achievements have been made through replacing porous carbon by graphite [10] or non-porous activated soft carbon (NPASC) electrodes in capacitors [11,12]. The developed asymmetric capacitors of activated carbon (AC)/graphite or NPASC/AC can hold the voltage as high as 3.5 V, whereas the symmetrical capacitor consisting of double NPASC electrodes even withstands the voltage of 4 V. Considering the shortcomings of NPASC such as the relatively low tap density and its somehow tedious preparation procedures, we attempted to substitute graphite for NPASC in a 4 V-capacitor. Since the performance of quaternary alkyl ammonium-intercalated graphite compounds as negative electrodes is not satisfactory [13], graphite was picked up as the positive electrode material in the 4 V-capacitor. Then the asymmetric configuration of NPASC/graphite was proposed. Because both the graphite positive and NPASC negative electrodes are subject to ions intercalation during charge–discharge cycles, the perceivable volume changes in both the electrodes are inevitable. In the previous study [14], we have processed raw mesophase carbon microbeads (MCMB) into a spherical NPASC appropriate for lessoning volume variations within a negative electrode. Here the graphitized MCMB was adopted as the positive material for a similar reason. This kind of spherical graphite with optimized conditions such as high tap density, small surface area, suitable crystallinity, etc., has already become successfully commercialized in the community of lithium-ion batteries. In this paper, an asymmetric dual-MCMB capacitor free of metal ions was constructed and its performance was tested. The electrochemical storage behavior at the negative electrode of activated MCMB was investigated.

2. Experimental

2.1. Materials

Raw MCMB was obtained from Beiterui Co. Ltd. It was carbonized and activated following the procedures as described in a previous study [14] Then the activated MCMB was heated in the atmosphere of hydrogen/nitrogen mixture (volume ratio 1:9) at 800 °C for 2 h to remove some oxygen functional groups, which may be catalytic for the electrolyte decompositions [15].The resultant MCMB was abbreviated as AMCMB and employed as a negative electrode material.

Graphitized MCMB (designated as GMCMB) also came from Beiterui Co. Ltd. It had been heated at the high temperatures over 2800 °C. Complimentary carbon electrode materials included activated carbon (PW15M13130 from Kureha Co. Ltd.) and artificial graphite (KS-6 from Timcal Co. Ltd.), whose physical properties have been described in the past reports [10,16].

2.2. Characterization

The morphological features of AMCMB and GMCMB were observed by field emission scanning electron microscopy (SEM, Philips XL 30) at an accelerating voltage of 10 kV. The porous structures were analyzed by N_2 adsorption/desorption at 77 K (Micromeritics ASAP2020, USA). The SSA was obtained using the Brunauer–Emmett–Teller (BET) method and the pore size distribution was calculated by the differential functional theory (DFT) analysis method. Thermal gravity analysis (TG) and differential thermal gravity (DTG) (STA 449 F3 Jupiter, NETZSCH) were carried out in the temperature range of 50–1000 °C in nitrogen phenomenon at a heating rate of 10 °C min^{-1}. The crystal structure changes of AMCMB before and after the first cycle of galvanostatic charge–discharge were measured by X-ray diffraction (XRD, a Bruker D8 Advance with Cu K at 1.5418 Å). All Raman spectra were measured by a Jobin Yvon/HORIBA LabRam ARAMIS Raman spectrometer equipped with a HeNe laser (633 nm). The typical exposure time for each measurement in this study was 30 s with one time accumulation.

2.3. Electrochemical measurements

The electrode materials were mixed with TAB (teflonized acetylene black, conductive binder) at the weight ratios of 2 to 1 and then pressed on the aluminum mesh as the current collector. The weight ratio of positive to negative active materials was 1:1. The used electrolyte in this study was 1.5 M triethylmethylammonium tetrafluoroborate ($TEMABF_4$) dissolved in propylene carbonate (PC). The galvanostatic charge–discharge test was run at the constant current density of 0.4 mA cm^{-2} in a two-electrode system (coin cell). The coin cell was assembled with current collector, electrode, separator (glass fiber filter) soaked with the electrolyte solution, electrode, and current collector in sequence as a sandwich. Cyclic voltammetry (CV) and electrochemical impedance spectroscopy (EIS) of electrode materials was measured by a three-electrode system, in which a large Pt sheet worked as a counter electrode while a heavy AC acted as a reference electrode. Unless specified otherwise, the scan rate is 0.1 mV s^{-1}.The assembling of two and three-electrode systems was carried out in a glove box with Ar atmosphere (water content < 0.5 PPM, oxygen content < 0.5 PPM). The cut-off voltages of AMCMB/GMCMB, AC/graphite, AC/AC cells were 0–4 V, 0–3.5 V, and 0–2.7 V, respectively. Charge storage ability of the total capacitor (coin cell) was expressed in the terms of capacity (mAh g^{-1}). The capacity values were calculated according to the following formula: $Q = IT/w_+$ (I, constant current (mA); T, the time for charge or discharge between cut-off voltages (h); w_+, the weight of positive electrode (g)).

3. Results and discussion

Fig. 1 shows the scanning electron microscopy (SEM) images of AMCMB (a, b) and GMCMB (c, d) in different dimensions.

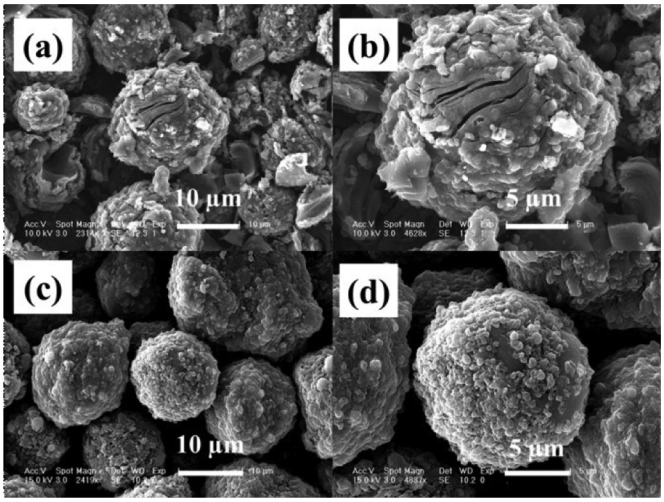

Fig. 1. The SEM images of AMCMB (a, b) and GMCMB (c, d).

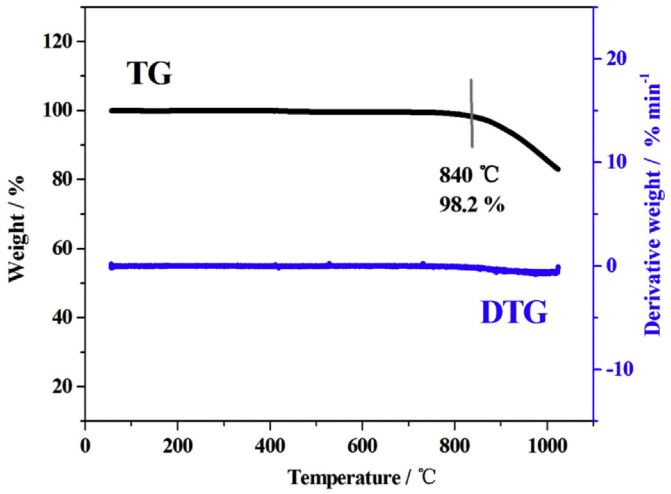

Fig. 3. TG and DTG curves of AMCMB.

The sphere shape of GMCMB keep integrated after a series of treatment (Fig.1(a)) and the crevices in the spheres are visible (Fig. 1(b)). The GMCMB is surface-rugged spherical particles with the average diameter of 15–20 μm, as showed in Fig. 1(c) and (d). Fig. 2(a) displays the N_2 adsorption/desorption isotherm curve of AMCMB, which is essentially characteristic of type II for a non-porous adsorbent. Besides, an indistinct type H4 hysteresis loop can be identified at the relative pressure $P/P_0 = 0.5–0.9$ and it is the feature of slit pores. The DFT pore size distribution of AMCMB is given in Fig. 2(b) and the cumulative pore volume is only 0.036 $cm^3\ g^{-1}$. Compared with the activated MCMB sample in the previous study [14], AMCMB here has a lower B. E. T. specific surface area (SSA) value of 24.48 $m^2\ g^{-1}$ and a larger tap density of 0.794 g cm^{-3}. The lower SSA may decrease the opportunity of electrolyte decompositions at the outer surface of AMCMB and guarantee more closed pore spaces for cations intercalation to foster the effect of "electrochemical activation". In addition, a larger tap density is very necessary to gain larger volumetric capacitance and higher energy density. TG and DTG curves in Fig. 3 justify the thermal stability and purity of AMCMB. AMCMB can hold 98.2% weight even at the high temperature of 840 °C. The DTG curve is almost a straight line, which notes very few subsidiary reactions from impurities.

Fig. 4 depicts the potential profiles of AMCM negative and GMCMB positive electrodes against a heavy AC reference electrode, respectively, during the first three cycles of galvanostatic charge–discharge of an AMCMB/GMCMB capacitor. In the initial charge curve, the total cell voltage of the capacitor at first rises very fast from the open circuit voltage (about 0.8 V) to 3.25 V, and the charge capacity in this section is less than 5 mAh g^{-1}. Accordingly, both the potentials of the GMCB positive and AMCB negative electrodes change drastically which means that their SSA are too small to adsorb many ions. From 3.36 V to the cut-off voltage of 4.0 V, the charge capacity of the full capacitor expands remarkably with the slow rising pace of total cell voltage. The knee point at 3.36 V in the initial charge curve of an AMCMB/GMCMB capacitor corresponds to two inflexion points simultaneously emerging in the potential profiles of AMCMB negative and the GMCMB positive electrodes, respectively; the former at −1.63 V while the latter at 1.73 V against the AC reference electrode. Then considerable amounts of ions start

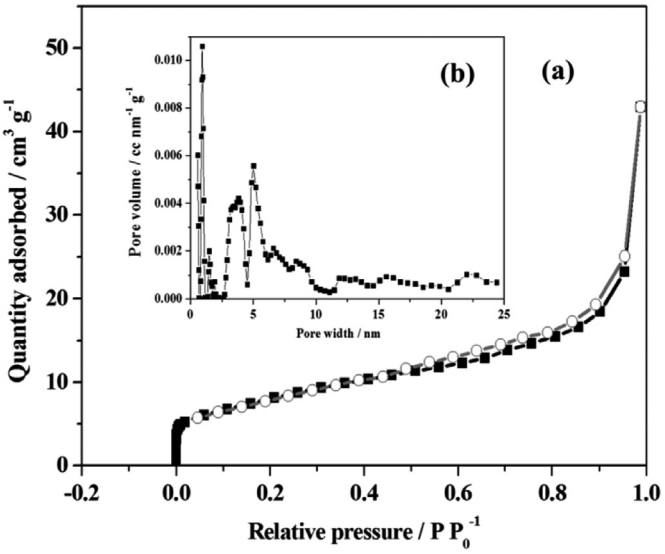

Fig. 2. N_2 adsorption–desorption isotherm (a) and DFT pore size distribution (b) of AMCMB.

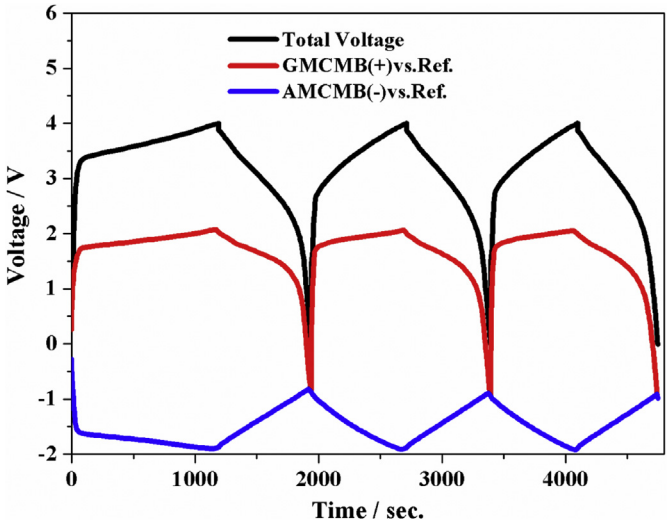

Fig. 4. The first three cycles of galvanostatic charge–discharge curves of a AMCMB/GMCMB capacitor.

to intercalate into both electrodes and these potential profiles turn to plateaus. The cations intercalation into the AMCMB negative electrode in the first charge process is an irreversible "electrochemical activation" [14], whereas the anion intercalation into GMCMB is nearly reversible, as compared with their modes in the subsequent charge–discharge cycles. When the total cell voltage of an AMCMB/GMCMB capacitor reaches 4.0 V, the potential of the AMCMB negative electrode touches down to the bottom value of −1.93 V (about 1.07 V vs. Li/Li^+), while the potential of GMCMB positive electrode climbs up to the ceiling value of 2.07 V (about 5.07 V vs. Li/Li^+). The bottom potential at −1.93 V against an AC reference electrode may be a delicate borderline of AMCMB electrode's cathodic stability, as in the case of a NPASC/AC capacitor approaching the cell voltage of 3.5 V [14]. On the other hand, the ceiling potential at 2.07 V against an AC reference electrode appears a limit of GMCMB electrode's anodic stability, similar to the occasion of AC/graphite capacitors [10,17]. The curves in the second and third cycles are almost the same but differ from the first cycle. The knee points in the charge curve of the capacitor shift to 2.67 V, which responds to only one inflexion point at 1.73 V in the potential profile of GMCMB positive electrode. On the contrary, the potential profile of the AMCMB negative electrode after the first charge becomes capacitive-like straight lines.

From the preliminary analysis on potential profiles, we realized that the irreversible "electrochemical activation" of AMCMB during the initial charge process is a key issue. Therefore, we carried out different investigations to characterize the influence of "electrochemical activation". XRD patterns of an AMCMB electrode before and after the initial charge–discharge are showed in Fig. 5. After the first cycle of charge–discharge process, the (002) diffraction peak shifts to a lower angle and becomes a little sharper. These changes testify that the interlayer spaces between adjacent graphene layers in the AMCMB became wider and its crystal structure gets more ordered after the "electrochemical activation". This tendency is in good agreement with the HRTEM (high resolution transmission electron microscope) results [14]. In contrast, Raman spectra of MCMB electrodes hint that the "electrochemical activation" may destruct the graphite crystal structure on the surface of AMCMB. As shown in Fig. 6, there are two peaks at about 1580 and 1360 cm^{-1} in each Raman spectrum. The former band (G band) is ascribed to Raman active E^2_{g2} mode of graphite lattice vibration, whereas the latter band (D band) is assigned to A1g mode, which comes from some kinds of disorders and defects in graphite crystal structure

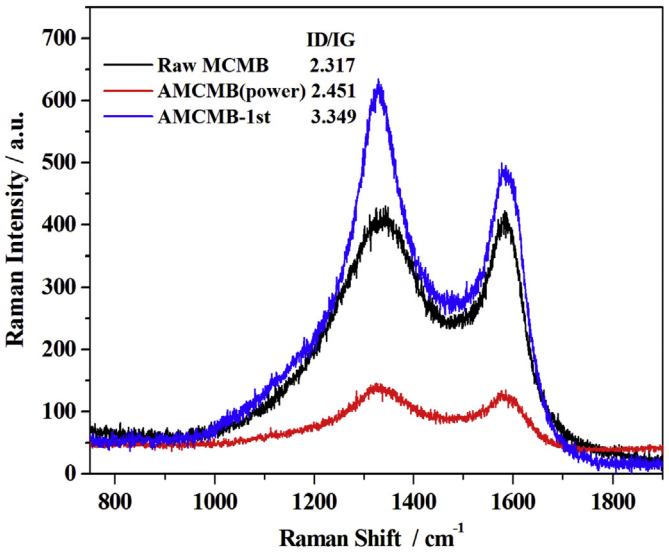

Fig. 6. Raman spectra of raw MCMB, AMCMB power and the AMCMB electrode in an AMCMB/GMCMB capacitor after the 1st cycle of galvanostatic charge–discharge test.

[18]. The intensity ratio of D to G band is an important parameter evaluating the disorder degree of carbon surface. After the first cycle charge–discharge, this parameter increases apparently. This fact seems to disagree with *ex situ* XRD and TEM results, which implies that the arrangement of carbon lamellas inside AMCMB particles becomes more ordered after the "electrochemical activation". However, these conflicting phenomena are actually relevant because the volume expansion of AMCMB particles during the "electrochemical activation" inevitably generates more cracks on the surface.

This "electrochemical activation" of AMCMB has also been studied by CV test as shown in Fig. 7. The scan potential range is from open circuit voltage (OCV) to −1.93 V. In the initial cycle, the cathodic current remains dormant at first in the potential region between the OCV and −1.3 V, then it jumps up abruptly with the potential sweep to the negative direction. Then there are two cathodic peaks can be clearly observed in the potential range

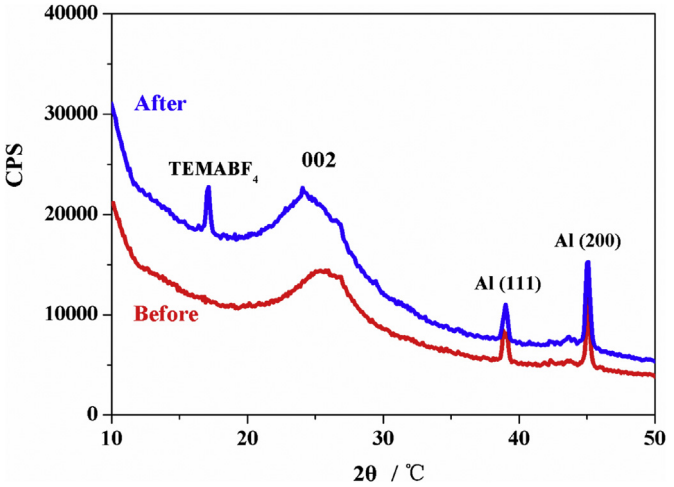

Fig. 5. XRD patterns of the AMCMB electrode in an AMCMB/GMCMB capacitor before and after the initial charge–discharge test.

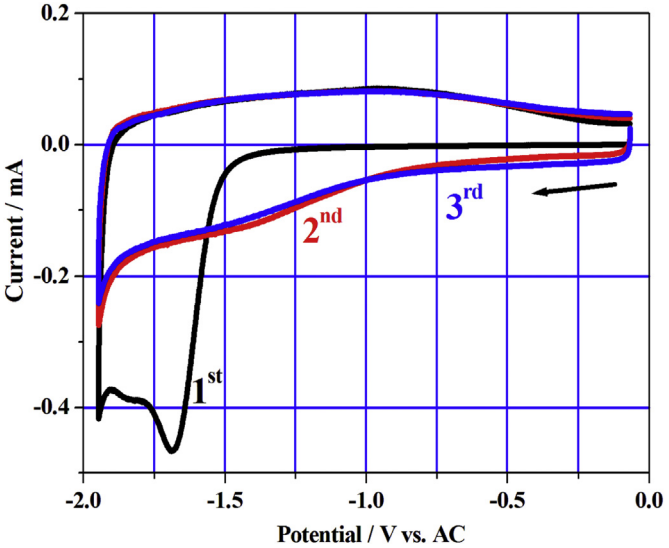

Fig. 7. The first three cycles of cyclic voltammograms for AMCMB in the potential range from the O.C.V. to 1.93 V with respect to the AC reference electrode.

between −1.3 V and −1.93 V. One appears at the cut-off voltage −1.93 V, and the other at about −1.68 V. The former peak still occurs in the next two cycles, so it may relate to a reversible electrochemical process, probably the cation insertion into AMCMB. The latter peak in fact coincides with the bent point at −1.63 V in the potential profile of AMCMB (Fig. 4), and it vanishes in the subsequent cycles. This peak stands for the main step of "electrochemical activation". It involves not only the irreversible alignment of carbon layers in AMCMB during the cations intercalation, but also some cathodic decomposition of electrolyte solutions (principally the organic solvent). After the first-cycle cathodic scan, the area surrounded by the CV curves bulges, which means more capacitance delivered from the AMCMB electrode. Moreover, the CV curves for the second and third cycles almost overlap completely, which verifies the high reversibility of AMCMB in the potential range after the "electrochemical activation".

The electrochemical activation effect was further verified by EIS experiments of the AMCMB negative electrode before and after the first cycle of CV test in the frequency region of 10^{-3} Hz and 10^{6} Hz at OCV. Fig. 8 shows the Nyquist plots (0.013 Hz was intercepted as the minimum frequency) of experimental impedance data and fitted data with a loop in high frequency region and a sloped line at low frequency region. The equivalent circuit used for fitting is $R_e(Q(R_{ct}Z_w))C_l$ and its schematic diagram showed in Fig. 8. The meanings of the five equivalent elements here are simply introduced: R_e is the equivalent series resistance, R_{ct} is the charge transfer resistance, Z_w is the Warburg impedance, Q is the constant phase element (CPE) and C_l is the limited capacitance. R_e includes the resistance of electrolytes, the intrinsic resistance of the electrode material and the resistance at electrode materials/current collector interface [19]. R_{ct} corresponding to the diameter of the semicircle in the high frequency region represents the kinetic resistance of charge transfer when the Faradaic reactions occur. Z_w is related to the slope of 45° part of the Nyquist plots in the middle frequency region, which is the impedance of the diffusion controlling process in the electrolyte. C_l is the limited capacitance. The double electric layer at the electrode/electrolyte boundary usually equals an EDLC, but it almost deviates a pure one because of dispersion effect. The equivalent element denoted this part is CPE (Q). Its impedance is defined as:

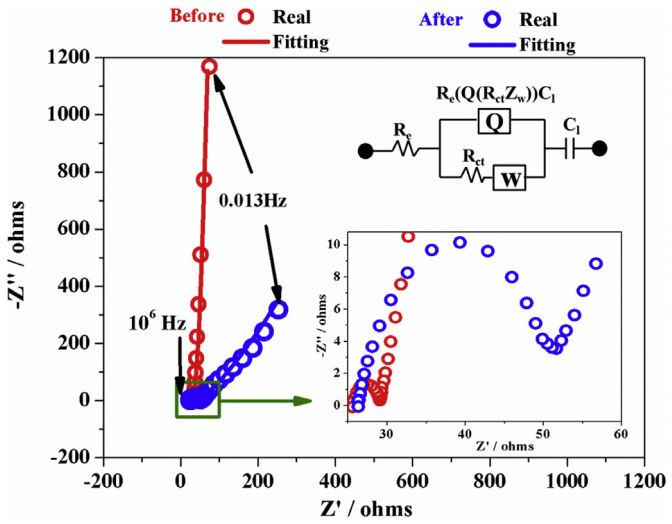

Fig. 8. Nyquist plots of experimental impedance data and fitted date of the AMCMB negative electrode before and after the first cycle CV test at OCV. Two insets are the equivalent circuit model for impedance analysis and the expanded part in the region of high frequency respectively.

$$Z_Q = [Y_0(j\omega)^n]^{-1} \quad (1)$$

leading to

$$Z'_Q = [Y_0(\omega)^n]^{-1}\cos(n\pi/2) \quad (2)$$

$$Z''_Q = [Y_0(\omega)^n]^{-1}\sin(n\pi/2) \quad (3)$$

where the dimension unit of Y_0 is 1 S cm^{-2} s^{-n} and it is a constant independently on frequency, n is an exponent with the value between −1 and 1. When $n = -1$, the CPE is a pure induce; $n = 0$, the CPE is a pure resistor; $n = 1$, the CPE is a pure capacitor; $0 < |n| < 1$, the CPE is Q. In the experiment of before and after the first cycle of CV test, the value of n changes from 1 to 0.8. It means the CPE behaves like a pure capacitor before the electrochemical activation. But after that, the behavior of the CPE deviates from a pure capacitor for the ions intercalation/deintercalation mechanism partly or totally in place of the adsorption/desorption in the AMCMB electrode. Table 1 lists the value of each element in the equivalent circuit calculated by the complex nonlinear least-squares (CNLS) method.

From the inset of expanded part of Nyquist plots at high frequency region, the value of R_e almost keeps steady before and after the first cycle of CV test, so the AMCMB material was surrounded by a stationary external environment. In the medium frequency, the loop with a larger amplitude forms after the first cycle CV test compared to before. Based on the stationary external environment of the AMCMB material, the increased impedance at real part comes from the kinetic resistance for electrolytes ions adsorbing into the new-born pore created via electrochemical activation. At low frequency region, the impedance at imaginary part shapely increases to form an almost vertical line with a phase angle 87.24° (showed in Fig. 9(a)) before CV test, which implies a capacitive behavior. While the phase angle decrease to 68.86° (showed in Fig. 9(a)) after the first cycle of CV test, and this change indicates that the capacitive behavior of AMCMB here accompanied with diffusion process. Bodes plots of impedance depending on frequency (in Fig. 9(b)) show an obvious decreasing on the impedance after the first cycle of CV test at low frequency, and it shows the positive aspect of electrochemical activation effect.

Fig. 10 compares the real part C′ (Fig. 10(a)) and the imaginary part C′′ (Fig. 10(b)) of capacitance dependent on frequency for the AMCMB negative electrode before and after the first cycle of CV test at OCV. The analysis method is referred to P. Simon [20]. At low frequency region, C′ corresponds to the capacitance of electrode material and C′′ corresponds to an energy loss by an irreversible process [20,21]. In Fig. 10(a), the value of C′ after the first cycle of CV test is about 4.5 times bigger than before at 10^{-3} Hz. So, it is again verified that the electrochemical activation has enlarged the capacitance. The frequency corresponding to the half of the maximum value of C′ is f_0, which is also the frequency corresponding to the peak appeared on the curve of C′′ vs. frequency showed in Fig. 10(b). The relaxation time constant, τ_0 (=$1/2\pi f_0$), can be calculated, and is the characterization of the transition of the

Table 1
The value of R_e, C(=Q, when $n = 1$), $Q(Y_0, n)$, R_{ct}, $Z_w(Y_0)$ and C_l calculated by CNLS using the fitting EIS data based on the relative equivalent circuit.

AMCMB	R_e (Ω)	C (F, $n = 1$)	Y_0 (S s^n)	n	R_{ct} (Ω)	Z_w (Y_0, S $s^{0.5}$)	C_l (F)
Before	25.43	3.57 * 10^{-6}	–	–	0.0342	0.0626	0.0113
After	26.31	–	9.10 * 10^{-6}	0.8	21.22	0.0127	0.0885

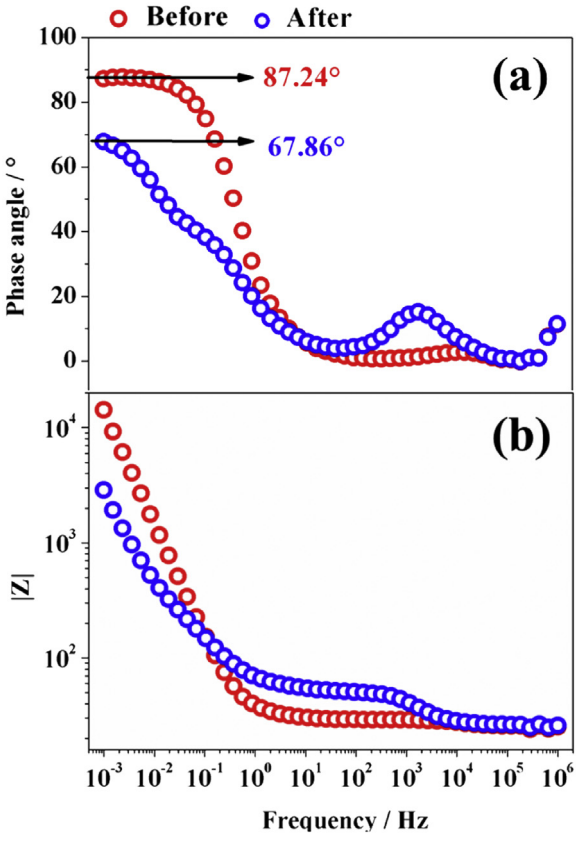

Fig. 9. Bode plots of (a) phase angle dependent on frequency, and (b) impedance dependent on frequency of the AMCMB negative electrode before and after the first cycle CV test at OCV.

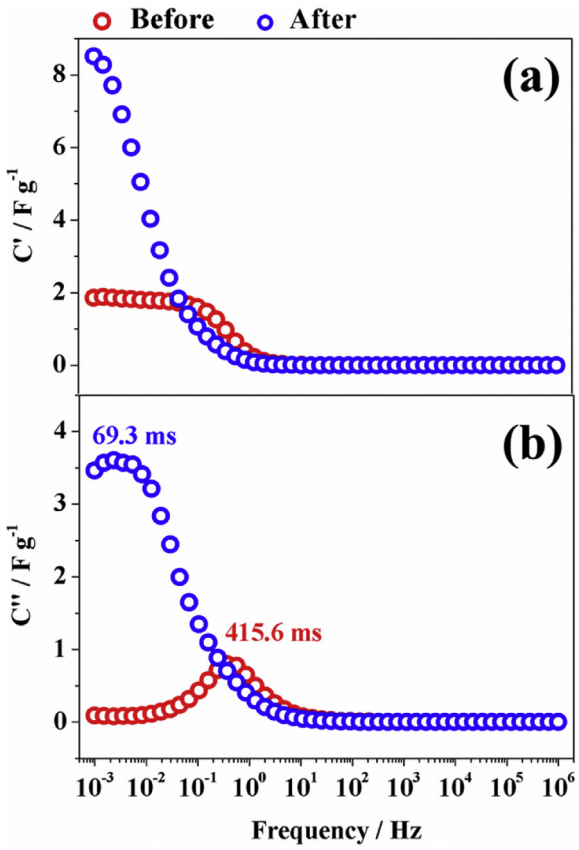

Fig. 10. The (a) real part and (b) imaginary part of capacitance dependent on frequency for the AMCMB negative electrode before and after the first cycle of CV test at OCV.

electrode material from purely resistive to purely capacitive behavior. When $f > 1/\tau_0$, it works as a pure resistor, and when $f < 1/\tau_0$, it works as a pure capacitor. The values of τ_0 calculated are 415.6 ms and 69.3 ms for before and after the first cycle of CV test, which indicates that AMCMB spend only one-sixth time to deliver the stored energy after electrochemical activation. It is strong evidence to proof that ions interposed into the limited pore have created and widen the micro-structure channels in AMCMB by electrochemical action.

Fig. 11 compares the initial galvanostatic charge–discharge curves of the capacitors using carbon electrode materials and the electrolyte of 1.5 M $TEMABF_4$ dissolved in PC. The discharge capacity values of the AMCMB/GMCMB and AMCMB/AC capacitors are much higher than the other two types of capacitors (AC/AC and AC/graphite). This comparison illustrates some superiority of AMCMB. Replacing AC by AMCMB (or NPASC) as a negative electrode in electrochemical capacitors may be an important technological progress to enhance the energy density since the porous carbon electrode materials have overwhelmed this community for over half a century [22,23]. On the other hand, the capacitors using a graphite positive electrode display bent discharge curves. This causes the sudden dropdown of cell voltage at the end of discharge and lacks enough capacity in the low voltage range (<2 V). So the significance of employing graphite positive electrode at first lies in its high potential.

Fig. 12 exhibits the CVs of each electrode confined within its working potential region in the above capacitors. The potential was recorded with respect to a heavy AC reference electrode. This figure helps identify the electrochemical behavior of each electrode in respective environments. Graphite positive electrodes (both GMCMB and KS-6) conform to the same charge storage manner with the reversible peaks standing for anions intercalation/de-intercalation. In contrast, AC electrodes, as either positive or negative one, furnish a rectangular shape characteristic of electric-double layer capacitance (EDLC). Nevertheless, it is hard to classify

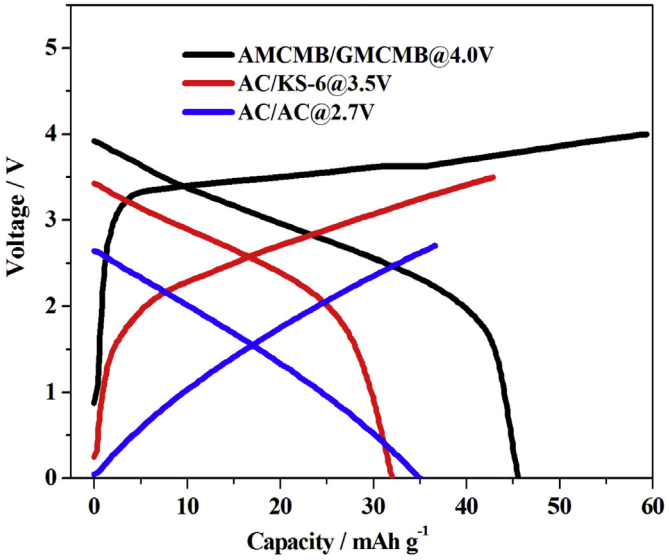

Fig. 11. Initial galvanostatic charge–discharge curves of the AMCMB/GMCMB, AC/graphite and AC/AC capacitors.

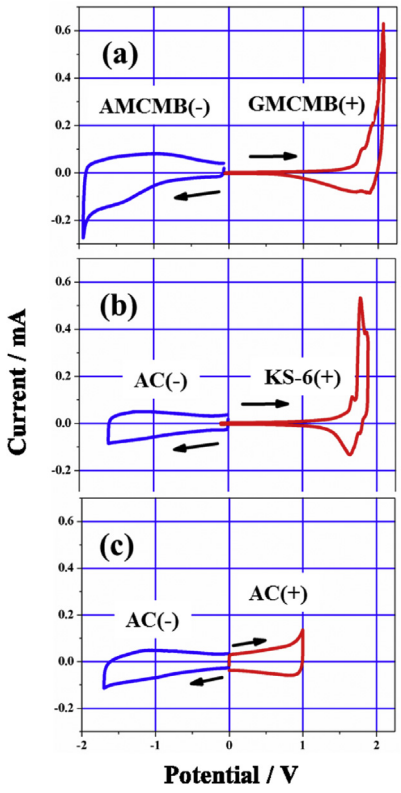

Fig. 12. Cyclic voltammograms of the positive and negative electrodes of three capacitors: (a) AMCMB/GMCMB, the cut-off voltages are about −2 to 0 V for AMCMB(−) and 0–2 V for GMCMB(+); (b) AC/graphite, the cut-off voltages are about −1.6 to 0 V for AC(−) and 0–1.9 V for graphite(+); (c) AC/AC, the cut-off voltages are about −1.7 to 0 V for AC(−) and 0–1 V for AC(+). 0 V is an approximation of O.C.V. in this CV test.

the fashion of AMCMB negative electrode into the above two types. In its appearance of CV, AMCMB behaves more like AC than graphite.

The Ragone plots of the four capacitors are compared in Fig. 13. The AMCMB/GMCMB capacitor wins the championship in the terms of both energy and power density. So elevating its working voltage is the most effective way to enhance both the energy and power density of a capacitor. Fig. 14 compares the cycle performance of these four capacitors. Although a high voltage constitutes a threat to the cycle performance in most cases, the AMCMB/GMCMB capacitor possesses excellent cycle ability not inferior to others at all.

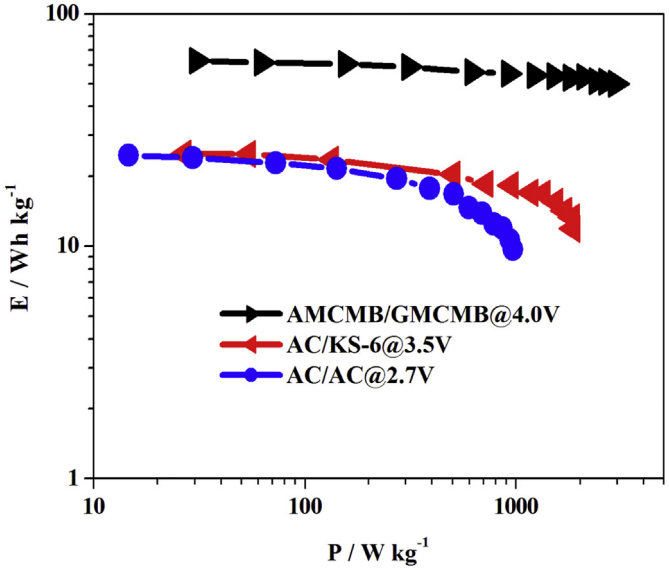

Fig. 13. Ragone plots of the AMCMB/GMCMB, GMCMB/GMCMB, AC/graphite and AC/AC capacitors.

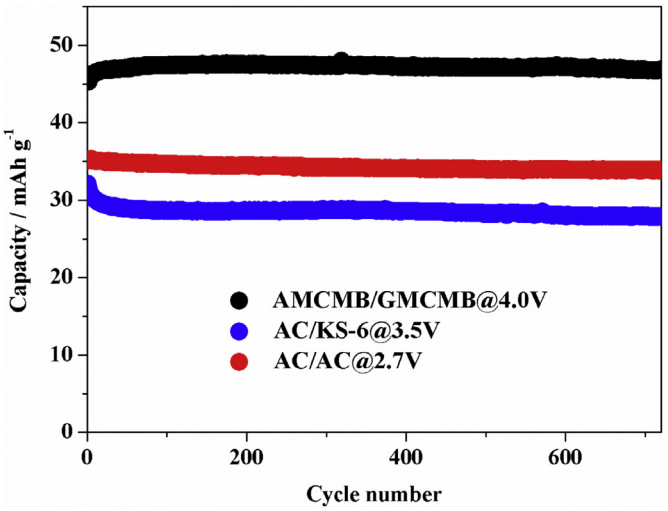

Fig. 14. Cycle performance of the AMCMB/GMCMB, AC/graphite and AC/AC capacitors.

4. Conclusion

The AMCMB/GMCMB capacitor using quaternary alkyl ammonium based organic electrolyte has made a 4 V metal-free electric energy storage device available. Heat treatment of AMCMB under hydrogen/nitrogen atmosphere is effective to improve its cathodic stability. The storage charge manner of AMCMB is different to either AC or graphite. The electrochemical activation of AMCMB in the first cycle is vital for its performance as a negative electrode. The AMCMB/GMCMB capacitor shows excellent performance in the terms of discharge capacity, energy density, power density and cycle ability, as compared with other “metal-free” capacitors.

Acknowledgments

This work was financially supported by National Natural Science Foundation of China (21173206), National Basic Research Program of China (2011CB935702), Scientific Research Foundation for the Returned Overseas Chinese Scholars and State Education Ministry (SRF for ROCS, SEM) and Hundred Talents Program of Chinese Academy of Sciences.

References

[1] K. .Naoi, Fuel Cell 5 (2010) 825.
[2] D. Cericola, R. Kötz, Electrochim. Acta 72 (2012) 1.
[3] G. Park, H. Nakamura, Y. Lee, M. Yoshio, J. Power Sources 189 (2009) 602.
[4] K. Wu, Y. Yang, Y. Liu, Y. Zhang, C. Wang, J. Xu, F. Ning, D. Wang, J. Power Sources 237 (2013) 285.
[5] Y.-B. He, B. Li, M. Liu, C. Zhang, W. Lv, C. Yang, J. Li, H. Du, B. Zhang, Q.-H. Yang, J.-K, Kim, F. Kang, Sci. Rep 2 (2012) 913, http://dx.doi.org/10.1038/srep00913.
[6] H. Wang, M. Yoshio, J. Power Sources 195 (2010) 1263.
[7] A. Laheäär, A. Jänes, E. Lust, Electrochim. Acta 56 (2011) 9048.
[8] T. Morimoto, K. Hiratsuka, Y. Sanada, K. Kurihara, J. Power Sources 60 (1996) 239.
[9] M. Hahn, A. Würsig, R. Gallay, P. Novák, R. Kötz, Electrochem. Commun. 7 (2005) 925.

[10] H. Wang, M. Yoshio, A.K. Thapa, H. Nakamura, J. Power Sources 169 (2007) 375.
[11] M. Takeuchi, K. Koike, T. Maruyama, A. Mogami, M. Okamura, Electrochemistry 66 (1998) 1311.
[12] M. Takeuchi, T. Maruyama, K. Koike, A. Mogami, M. Okamura, Electrochemistry 69 (2001) 487.
[13] H. Wang, M. Yoshio, J. Power Sources 200 (2012) 108.
[14] C. Zheng, J. Gao, M. Yoshio, L. Qi, H. Wang, J. Power Sources 231 (2013) 29.
[15] K. Hiratsuka, Y. Sanada, T. Morimoto, K. Kurihara, Electrochemistry 59 (1991) 607.
[16] H. Wang, M. Yoshio, Electrochem. Commun. 8 (2006) 1481.
[17] H. Wang, M. Yoshio, J. Power Sources 177 (2008) 681.
[18] E. Tuinstra, J.L. Koenig, J. Chem. Phys. 53 (1970) 1126.
[19] J. Gamby, P. Taberna, P. Simon, J. Fauvarque, M. Chesneau, J. Power Sources 101 (2001) 109.
[20] P. Taberna, P. Simon, J. Fauvarque, J. Electrochem. Soc. 150 (2003) A292.
[21] V. Ganesh, S. Pitchumani, V. Lakshminarayanan, J. Power Sources 158 (2006) 1523.
[22] H.I. Becker, U.S. Patent 2,800,616, 1957.
[23] R.A. Rightmire, U.S. Patent 3,288,641, 1966.